General Design Equations, Small-Sized Impedance Transformers, and Their Application to Small-Sized Three-Port 3-dB Power Dividers

Hee-Ran Ahn, *Senior Member, IEEE,* and Ingo Wolff, *Fellow, IEEE*

***Abstract*—In this paper, design equations for three-port power dividers have been derived. These design equations are available for both arbitrary power divisions and arbitrary termination impedances, and many sets of design equations are possible. Therefore, the design equations may be called *general design equations* and an arbitrary design impedance A is introduced to describe them. On the basis of the derived general design equations, a coplanar three-port power divider with a power split ratio (3 dB) terminated by 50, 60, and 70 Ω is designed with $A = 33.33\ \Omega$, so that a commercially available resistor 100 Ω can be used for the isolation resistance. Additionally, to reduce the size of transmission-line impedance transformers, two types of small-sized impedance transformers are designed, named a constant VSWR-type transmission-line impedance transformer (CVT) and a constant conductance-type transmission-line impedance transformer (CCT) and compared with conventional reduced-sized impedance transformers. These impedance transformers are designed in the low-Q region on the Smith chart. Therefore, they show wide-band properties. To make sure that the derived design equations of CVTs and CCTs are reasonable, four 1.6 : 1 impedance transformers, CVT 20°, CVT 30°, CCT 15°, and CCT 20° have been fabricated in microstrip technology and measured. The measured results show the expected tendency. Based on the CVTs and CCTs, small-sized three-port 3-dB power dividers are constructed and named a constant VSWR-type three-port 3-dB power divider (CVT3PD) and a constant conductance-type three-port 3-dB power divider (CCT3PD). For the CVT3PD and CCT3PD, perfect isolation conditions are derived, and it is shown that the perfect isolation circuit (I.C) must be composed of resistance combined with capacitance or inductance in the case that the length of transmission lines is not $\lambda/4$. These I.Cs are quite different from conventional ones composed of only resistance. Finally, on the basis of the derived perfect isolation impedance, CVT3PD and CCT3PD are designed and simulated, giving the possibility that a CCT3PD can be realized with the electrical length 15.30° of the transmission lines.**

***Index Terms*—General design equations of three-port power dividers, small-sized impedance transformers (CVTs and CCTs), small-sized three-port 3-dB power dividers (CVT3PDs and CCT3PDs).**

I. Introduction

THREE-PORT power dividers are useful microwave devices for phased-array antennas, power amplifiers, mixers, or active circulators. Hybrid power dividers are generally classified by two groups: four- and three-port power dividers. The three-port power divider originated from Wilkinson [1] who described a circularly symmetric power divider, which split a signal into n-equiphase–equiamplitude signals with an even or odd number of n. With $n = 2$, Wilkinson's power divider could be a three-port power divider achieving a perfect isolation at one frequency. In 1965, Parad and Moynihan [2] presented a three-port power divider with in-phase and arbitrary amplitude difference between two outputs. Perfect three-port hybrid property was again achieved at one frequency. In 1968, Cohn [3] presented a class of broad-band three-port hybrids with high isolation between two outputs and good matching at all ports.

In 1971, Ekinge [4] described a three-port hybrid, which consisted of n sections in cascade with each section composed of two coupled lossless transmission lines of electrical length Θ and an intermediate resistor, which seemed to be similar to that of Cohn's [3]. However, Cohn treated the equal power split three-port hybrids, whereas Ekinge [4] treated the arbitrary power split three-port hybrids. Since that time, the studies on three-port hybrids have been continued [5]–[8]. However, they just focus on symmetrical structures where even- and odd-mode excitation analyses are available. In the case that power dividers are used with active and/or passive elements, additional matching networks are necessary to obtain the desired output performances. If these power dividers are terminated by arbitrary impedances, the total size of integrated microwave circuits may be reduced. Asymmetric power dividers were first proposed by Ahn *et al.* for ring hybrids [9], [10], branch-line hybrids [11], [12], and asymmetric three-port power dividers [13]. However, these three-port power dividers are limited to three-port 3-dB power dividers terminated by different impedances. Additionally, since only resistors have been utilized for optimal isolation between two ports, intensive optimization methods have been the only way to derive the isolation resistances in the case that the length of transmission lines is not $\lambda/4$ [3], [4], [7]. Very recently, a perfect isolation condition was derived by Ahn and Wolff [13]. However, this isolation condition is also effective in the case of $\lambda/4$ transmission lines.

In this paper, design equations are derived for three-port power dividers with both arbitrary termination impedances and arbitrary amplitude difference between two output signals. To derive these design equations, an arbitrary design impedance A, whose value is positive and arbitrary, is introduced. Therefore, according to the arbitrary values of A, many sets of design

Manuscript received August 31, 2000.

The authors are with the Department of Electrical Engineering, Gergard-Mercator University, D-47048 Duisburg, Germany (e-mail: ahn@ate.uni-duisburg.de).

Publisher Item Identifier S 0018-9480(01)05048-7.

equations are available. They are, therefore, called general design equations. These general design equations were very briefly discussed in [14], and a three-port power divider is simulated with $A = 39.5\ \Omega$ based on the derived general design equations. When compared to a conventional three-port power divider [2] in the case of a power split ratio (3 dB) and all termination impedances 50 Ω's, the results show that the three-port power divider with $A = 39.5\ \Omega$ is, in general, better than those of the conventional three-port power divider in terms of bandwidths. On the basis of the derived general design equations, a uniplanar three-port power divider terminated by 50, 60, and 70 Ω is designed with a power split ratio (3 dB) and the arbitrary design impedance A is determined as 33.333 Ω to adjust the isolation resistance to a commercially available resistor. In this way, the arbitrary design-impedance A may be determined for a special purpose, but the A should be determined for the optimum property. For this reason, the method to determine A is presented in terms of bandwidths. In addition, to reduce the size of the transmission-line impedance transformer, formulas have been derived for the graphical method [15] to match a complex load to a real reference load. Using the derived formulas, two small-sized impedance transformers are designed and named a constant VSWR-type transmission-line impedance transformer (CVT) and a constant conductance-type transmission-line impedance transformer (CCT). Since these two types of small-sized transformers are designed in the low-Q region on the Smith chart, they show wider bandwidths compared to any conventional reduced-sized transformers [16]. For small-sized three-port 3-dB power dividers, two types of constant VSWR-type three-port 3-dB power divider (CVT3PD) and constant conductance-type three-port 3-dB power divider (CCT3PD) are constructed based on the CVTs and the CCTs, and the perfect isolation conditions for the CVT3PD and CCT3PD are derived and simulated. It is proven that the isolation circuit (I.C) must be composed of resistance combined with capacitance or inductance for the perfect isolation when the length of transmission lines is not $\lambda/4$. Finally, two types of small-sized CVT3PD and CCT3PD are designed and their frequency responses are simulated. One of the CCT3PDs gives the possibility that a three-port 3-dB power divider can be realized with two transmission lines (each electrical length 15.3°) together with a capacitor and a resistor.

This paper is organized as follows. General design equations are discussed in Section II. Section III describes how to get small-sized transmission-line impedance transformers. Section IV explains how to derive perfect isolation conditions and how to design small-sized CVT3PDs and CVT3PDs. Finally, applications to microwave integrated circuits (MICs) are discussed in Section V.

II. General Design Equations

A. Analyses

A three-port power divider is depicted in Fig. 1(a). This power divider consists of two pairs of transmission lines and a bridging I.C between port $i②$ and $i③$ and is terminated by arbitrary impedances R_a, R_b, and R_c. The length of one pair of transmission lines with the characteristic impedances Z_{02} and Z_{03} is Θ_1 and

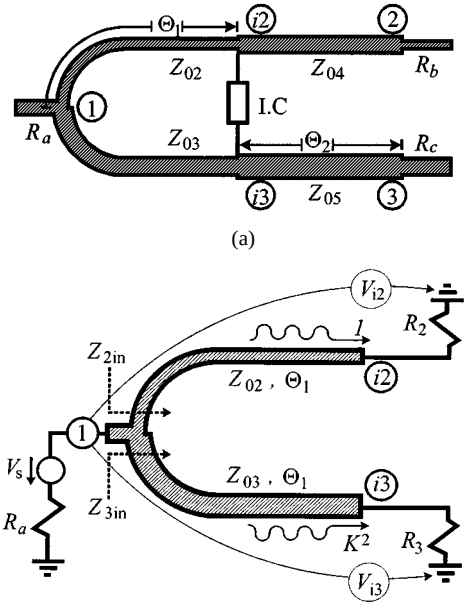

Fig. 1. Three-port power divider with arbitrary power divisions terminated by arbitrary impedances. (a) Whole circuit of the three-port power divider. (b) An equivalent circuit when the power is excited at port ①.

that of another pair with Z_{04} and Z_{05} is Θ_2 to satisfy the original definition that two output signals are in phase. When the power is excited at port ①, the equivalent circuit may be drawn as shown in Fig. 1(b). For the circuit in Fig. 1(b), if the power excited at port ① is split between two ports, $i②$ and $i③$ with the ratio 1: K^2, the input impedance $Z_{2\text{in}}$ looking into the transmission line with Z_{02} is $R_a(1+K^2)$ and $Z_{3\text{in}}$ is $R_a(1+K^2)/K^2$ as asymmetric ring hybrids [9], [10]. Therefore, both asymmetric ring hybrids and three-port power dividers have the same characteristics. The power excited at port ① is divided into two output ports, $i②$ and $i③$ and the two signals arriving at ports $i②$ and $i③$ are in phase and the voltage V_{i2} (from port ① via port $i②$ to ground) is equal to that of V_{i3} (from port ① via port $i③$ to ground) in Fig. 1(b). Since the ratio of $Z_{2\text{in}}$ to $Z_{3\text{in}}$ is K^2, the current entering into the transmission line with Z_{03} is K^2 times that with Z_{02}. The I.C is necessary for the output-port match and isolation. However, for asymmetric ring hybrids, the characteristic impedance Z_{02} is not related with Z_{03}. Since the I.C consists of two other lossless transmission lines and is not related with the circuit in Fig. 1(b), the isolation characteristics may be defined a forward isolation. R_2 and R_3 are independent of the power split ratio. The input reflection coefficient S_{11} is not a function of S_{22} and S_{33}, where S_{22} and S_{33} are reflected scattering parameters at port ② and ③, respectively. For three-port power dividers, the ratio of R_2 to R_3 should be K^2 to satisfy the condition that the voltage at port $i②$ is equal to that at port $i③$. Since the I.C is related with two transmission lines with Z_{02}, Z_{03}, and the termination impedance R_a, the isolation characteristics may be defined a backward isolation. S_{11} is a function of S_{22} and S_{33} [13].

The ratio of R_2 toR_3 in Fig. 1(b) yields

$$R_2 = K^2 A \tag{1}$$

$$R_3 = A \tag{2}$$

where A is an arbitrary positive value with the unit Ω.

Depending on the value of A, many sets of R_2 and R_1 are available. Therefore A may be defined an arbitrary design impedance. Parad *et al.* [2] suggested $R_2 = KR_a$ and $R_3 = R_a/K$ as a trial value among many possible cases in (1) and (2). The transmission lines with Z_{02}, Z_{03}, Z_{04}, and Z_{05} are impedance transformers. Therefore, if $\Theta_1 = \Theta_2 = 90°$, they are

$$Z_{02} = \sqrt{AR_aK^2(1+K^2)} \tag{3}$$

$$Z_{03} = \sqrt{AR_a\frac{1+K^2}{K^2}} \tag{4}$$

$$Z_{04} = K\sqrt{AR_b} \tag{5}$$

$$Z_{05} = \sqrt{AR_c}. \tag{6}$$

The I.C in Fig. 1 consists only of resistance if $\Theta_1 = 90°$, but it will be shown later that the I.C is not directly related with R_2 and R_3 and generally consists of resistance combined with capacitance or inductance. In the case of $\Theta_1 = 90°$, the I.C consists of pure resistance and the resistance R_{es} gives

$$\text{I.C} \rightarrow R_{es} = A\left(1+K^2\right). \tag{7}$$

From (1)–(7), according to the values of A, many sets of design equations are available. Therefore, these design equations may be called general design equations of three-port power dividers. The design equations of the conventional three-port power divider [2] are only one set of the general design equations with $A = Z_0/K$ in the case of $R_a = R_b = R_c = Z_0$. Three-port power dividers are easily realized with microstrip lines, strip lines, coplanar wave guides, and so on, but commercially available resistors are limited for the realization of conventional three-port power dividers in MIC or hybrid integrated circuit (HIC) technology. However, a proper choice of the design impedance A allows three-port power dividers to be easily realized. When a power split ratio is 3 dB and all termination impedances are equally 50 Ω's in the case of a conventional three-port power divider, $A = 35.39\ \Omega$ and its corresponding data are $Z_{02} = 102.85\ \Omega$, $Z_{03} = 51.54\ \Omega$, $Z_{04} = 59.43\ \Omega$, $Z_{05} = 42.07\ \Omega$, and $R_{es} = 106.03\ \Omega$. On the other hand, under the same conditions (the power split ratio is 3 dB and all termination impedances are equally 50 Ω's), those of the three-port power divider with $A = 39.5\ \Omega$ are $Z_{02} = 108.6\ \Omega$, $Z_{03} = 54.45\ \Omega$, $Z_{04} = 62.775\ \Omega$, $Z_{05} = 44.44\ \Omega$, and $R_{es} = 118.3\ \Omega$. The two three-port power dividers have been simulated under ideal conditions and HP EEsof Series IV has been used as a simulator. They are designed at the center frequency of 3 GHz and the simulated results are plotted in Fig. 2. Matching frequency responses are described in Fig. 2(a) and power division and isolation frequency responses in Fig. 2(b), where the solid line performances are the simulated results of the three-port power divider with $A = 39.5\ \Omega$ and the dotted ones indicate those of the conventional three-port power divider. "DBm" denotes the results with decibels proposed by one set of general design equations and "DBp" denotes those described by [2]. The exact simulated results of the two power dividers are given in Table I. Perfect matching at each port and the perfect isolation appears

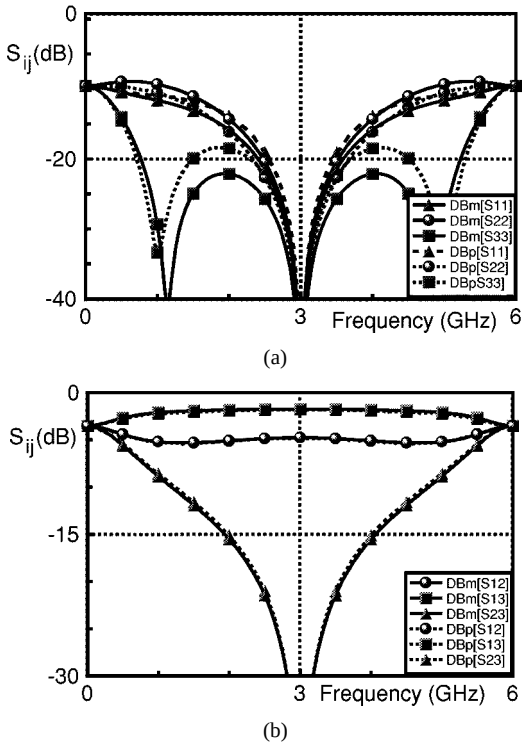

Fig. 2. Compared simulated results between a conventional three-port power divider and that with $A = 35.39\ \Omega$ (in both cases, a power split ratio (3 dB) and all termination impedances equally 50 Ω's). (a) Matching frequency responses. (b) Power divisions and isolation frequency responses.

TABLE I
COMPARED RESULTS BETWEEN TWO THREE-PORT POWER DIVIDERS WITH DIFFERENT VALUES OF "A" (ALL TERMINATION IMPEDANCES: 50 Ω's, POWER SPLIT RATIO: 3 dB, $K^2 = 1.995$, DESIGN CENTER FREQUENCY: 3 GHz)

	Simulated results using general design equations	Simulated results of a conventional power divider
A (Arbitrary design imp.)	39.5 Ω	35.39 Ω
Power divisions	$\|S_{21}\|$ = - 4.76 dB	$\|S_{21}\|$ = - 4.76 dB
	$\|S_{31}\|$ = - 1.76 dB	$\|S_{31}\|$ = - 1.76 dB
Matching	$\|S_{11}\|$ = - 118.2 dB	$\|S_{11}\|$ = - 91. 0 dB
	$\|S_{22}\|$ = - 96.16 dB	$\|S_{22}\|$ = - 78.16 dB
	$\|S_{33}\|$ = - 95.2 dB	$\|S_{33}\|$ = - 84.5 dB
Isolations	$\|S_{23}\|$ = -101.9 dB	$\|S_{23}\|$ = - 90.0 dB
Bandwidths less than -20dB in matching and isolations.	1.5 : 1 at port ① 1.4 : 1 at port ② 6.5 : 1 at port ③ 1.5 : 1 between port ② and port ③	1.3 : 1 at port ① 1.6 : 1 at port ② 1.6 : 1 at port ③ 1.45 : 1 between port ② and port ③

with the values of $|S_{11}| = -118.2$ dB, $|S_{22}| = -96.16$ dB, $|S_{33}| = -95.2$ dB, and $|S_{23}| = -101.8$ dB in the three-port power divider with $A = 39.5\ \Omega$. From the compared data in Table I, the frequency dependencies of the three-port power divider with $A = 39.5\ \Omega$ are, in general, better than those of the conventional three-port power divider in terms of bandwidths.

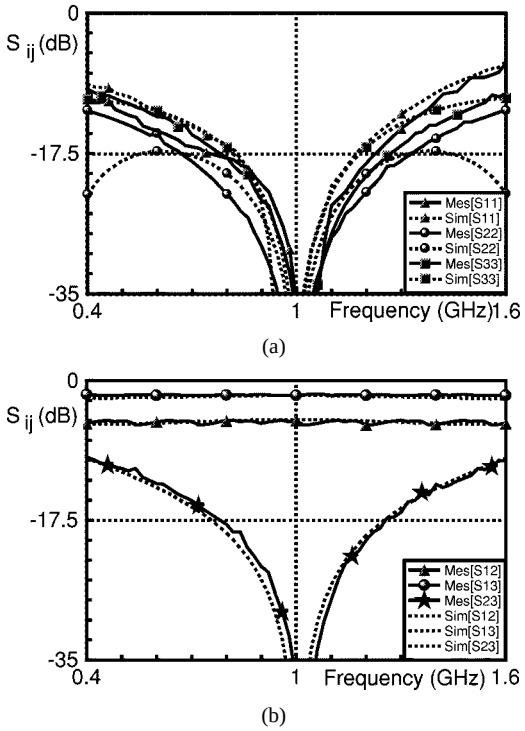

Fig. 3. Measured results of the uniplanar three-port power divider with the power split ratio (3 dB) and termination impedances 50, 60, and 70 Ω. (a) Matching frequency responses. (b) Power divisions and isolation frequency responses.

B. Coplanar Three-Port Power Divider Terminated by 50, 60, and 70 Ω

On the basis of the general design equations (1)–(7), a coplanar three-port power divider with the power split ratio (3 dB) terminated by 50, 60, and 70 Ω has been fabricated on an Al_2O_3 substrate ($\varepsilon_\gamma = 9.9$ and $h = 635$ μm). To adjust an isolation resistance to a commercially available resistor of 100 Ω, the arbitrary design impedance A is set to 33.33 Ω and all design values are $K^2 = 2$, $Z_{02} = 100\,\Omega$, $Z_{03} = 50\,\Omega$, $Z_{04} = 63.25\,\Omega$, $Z_{05} = 48.3\,\Omega$, and $R_{es} = 100\,\Omega$. This power divider is designed at the center frequency of 1 GHz and all measured results are plotted in Fig. 3. Matching frequency responses are described in Fig. 3(a) and power division and isolation frequency responses in Fig. 3(b), where the solid lines are the measured results and the dotted lines are the simulated ones. In the case of $K^2 = 2$, the power split ratio is 3 dB and the measured result of S_{31} and S_{21} are -1.84 and -4.8 dB at 1 GHz showing good agreements between simulated results of -1.7 and -4.7 dB. All-port measured matching and isolations are less than -35 dB within a relative bandwidth of 0.14 around 1 GHz.

C. How to Determine A

By the special purpose for realizing the isolation resistance with the commercial resistor of 100 Ω, the arbitrary design impedance A may be determined in the case of the uniplanar three-port power divider noted above. However, the realization of any value of resistance is, in general, not a big problem in the application of monolithic microwave integrated circuits (MMICs). The bandwidths of three-port power dividers are also limited by the worst property. In terms of bandwidths, the band of S_{11} less than -20 dB is 1.3 : 1, and the result is the worst case, as shown in Table I in the case of the conventional three-port power divider. Thus, the bandwidth of the conventional three-port power divider may be 1.3 : 1. Therefore, how to increase the bandwidth depends on determining the value of A. The transmission line with Z_{02} transforms the impedance $Z_{2\text{in}}$ into R_2, and $Z_{3\text{in}}$ is transformed into R_3 by the transmission line with Z_{03} in Fig. 1(b). Both of the impedance transformation ratios of $Z_{2\text{in}}$ to R_2 and $Z_{3\text{in}}$ to R_3 are equally

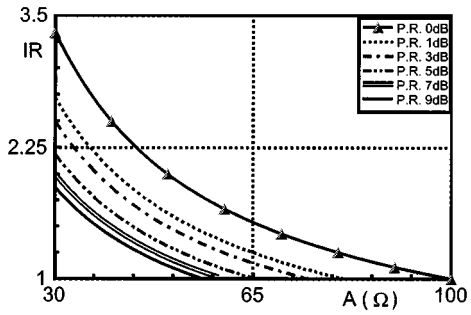

Fig. 4. Impedance transformation ratio IR_{1i2} depending on a power division ratio K^2 and an arbitrary design impedance A.

$$\mathrm{IR}_{1i3} = \mathrm{IR}_{1i2} = R_a \frac{1+K^2}{K^2 A} \tag{8}$$

where IR_{1i3} and IR_{1i2} are the impedance transformation ratios between the two ports. The impedance transformation ratios are not dependent on the termination impedances R_b and R_c, and are solely determined by R_a and K^2. Since the two impedance transformation ratios are always equal to each other, the power-division frequency responses show good performance in whole band, as shown in Figs. 2 and 3, and IR_{1i3} and IR_{1i2} determine the bandwidth of the reflection coefficient at port ① or S_{11}. When designing the three-port power dividers, the termination impedance R_a and the power split ratio K^2 are already given. Therefore, the choice of the arbitrary design impedance A plays an important part for increasing the bandwidth of three-port power dividers. Fig. 4 shows the relation between K^2, A, and IR_{1i3} when $R_a = 50\,\Omega$, $Z_{2\text{in}} \geq R_2$, and $Z_{3\text{in}} \geq R_3$. In this figure, "P. R." signifies a power split ratio K^2 in decibels. The results show that, as the design impedance A gets higher, the impedance transformation ratio IR comes close to one, and a three-port 3-dB power divider with "P. R. 0 dB" in this figures has the worst condition in terms of bandwidths of S_{11}. Since R_2 and R_3 give influence on S_{22} and S_{33}, as shown in Fig. 1(b), the determination of A is limited by how to design the next stage. Two transmission lines with Z_{04} and Z_{05} have no relation with each other. Therefore, two waves arriving at ports ② and ③ may be in a different phase, but if the length of the two transmission lines is 90°, the phase difference may be acceptable. Nevertheless, the smaller the difference in two impedance (admittance) transformation ratios IR_{i33} and IR_{i22}, the better performance may be expected. To determine the value of A for reducing the difference in two impedance transformation ratios

IR_{i33} and IR_{i22}, first find the value of A satisfying the minimum difference among four impedances R_2, R_b, R_3, and R_c, i.e.,

$$\min ||R_b - R_2| - |R_c - R_3||. \tag{9}$$

However, the value of A satisfying (9) does not guarantee the difference between IR_{i33} and IR_{i22} is minimum or zero. The value is just a initial value to decide $\mathrm{IR}_{i22} = R_2/R_b$ or R_b/R_2 and $\mathrm{IR}_{i33} = R_3/R_c$ or R_c/R_3. After determining both IR_{i33} and IR_{i22} greater than one, the difference is defined as

$$\mathrm{Diff} = \min |R_{i33} - R_{i22}|. \tag{10}$$

After calculating the value of A satisfying (10), compare the worse result among S_{22} and S_{33} with S_{11}. If S_{11} is better than the worse result, take the value of A. Otherwise, increase the A until S_{11} is about same as the worse result among S_{22} and S_{33}. In the case of a conventional three-port power divider with the power split ratio (3 dB) terminated by equal impedances of 50 Ω's, the value of A satisfying (10) is 35.39, which is exactly the same as that suggested by [2]. However, the bandwidth of S_{11} is not wider than that of S_{22} or S_{33} in the conventional three-port power divider case in Table I. Therefore, the design impedance A should be increased to improve the performance of S_{11}.

III. Small-Sized Transmission-Line Impedance Transformers

The most important design tool in microwave passive and active components is the concept of impedance matching. All values of impedances can be plotted in a reflection coefficient plane and those of passive component loads are $|\Gamma| \leq 1$, where Γ is a complex reflection coefficient. Therefore, a Smith chart has extensively been used to build matching circuits [17]. However, though the plane of the Smith chart expresses reflection coefficients of loads, not only are the coordinates written on the Smith chart load oriented, but the numbers on it are not also linear. Therefore, reading errors may easily be committed. In this paper, to reduce the size of transmission-line impedance transformers, a matching technique to match a complex load to a real impedance (admittance) with only one transmission line is needed. This matching technique was graphically [15] and theoretically [18] proposed. However, a formula for the length of the transformer line is thought not correct [18] and the graphical method [15] requires two times impedance (admittance) normalization to get the transformer line. In this process, reading errors are easily committed [19]. Also, the graphical method [15] was considered only if the complex load was located on the left-hand-side upper half-plane in the Smith chart.

In this paper, formulas for the transformer lines to match a complex load to a real reference load are mathematically derived and two types of small-sized transmission-line impedance transformers are constructed using the derived formulas. These small-sized transmission-line transformers will be very useful for the miniaturized microwave circuits, and the derived design equations will be utilized for matching circuit optimizations.

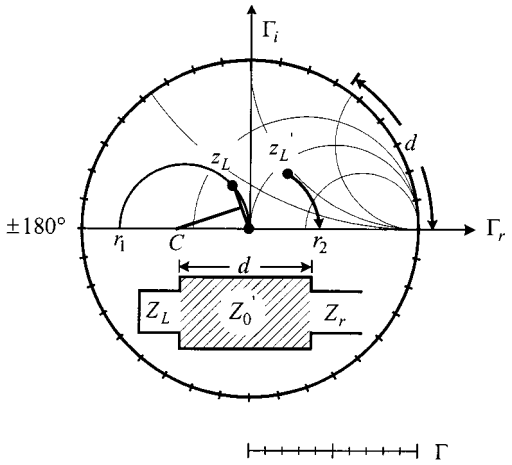

Fig. 5. Smith chart to get a transformer line to transform a complex load Z_L to a reference real load Z_r.

A. Mathematical Approach for Impedance Transformers

A transmission-line transformer to match a complex load Z_L to a real reference impedance Z_r is depicted in the lower part of the Smith chart, and the graphical procedure to get the transformer line with a characteristic impedance Z_0' and a length d is illustrated in the Smith chart of Fig. 5, where z_L is a complex load normalized to Z_r, $\sqrt{r_1}$ is a characteristic impedance Z_0' normalized to Z_r, C is the center of the circle passing through two points z_L and the center of the Smith chart, and z_L' is the complex load Z_L re-normalized to Z_0'. Through the relation of $\Gamma = (z_L - 1)/(z_L + 1)$, the real part Γ_r and the imaginary part Γ_i of Γ are derived as

$$\Gamma_r(r, x) = \frac{(r^2 - 1) + x^2}{(1 + r)^2 + x^2} \tag{11}$$

$$\Gamma_i(r, x) = \frac{2x}{(1 + r)^2 + x^2} \tag{12}$$

where r and x are a real and imaginary part of z_L, respectively. Since C is the center of the circle that passes through two points z_L and the center of the Smith chart, the perpendicular bisector of the line (from the center of the Smith chart) to z_L is projected onto the real axis, i.e., point C. The value at the point r_1 is two times that of point C. Therefore, the reflection coefficient at r_1 is

$$\Gamma_r(r, x)|r_1 = \frac{\left[\Gamma_r(r, x)|z_L\right]^2 + \left[\Gamma_i(r, x)|z_L\right]^2}{\Gamma_r(r, x)|z_L} \tag{13}$$

where $\Gamma_r(r, x)|z_L$ and $\Gamma_i(r, x)|z_L$ are the real and imaginary parts of the reflection coefficient at z_L, respectively. A formula for the impedance Z_0' based on (11) and (13) yields

$$\frac{Z_0'}{Z_r} = \sqrt{\frac{1 + \Gamma_r(r, x)|_{r_1}}{1 - \Gamma_r(r, x)|_{r_1}}}. \tag{14}$$

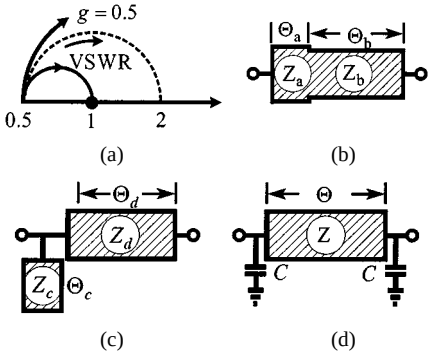

Fig. 6. Impedance transformers to transform a real impedance to a real reference impedance. (a) Part of the Smith chart (in the case of IR = 2). (b) CVT. (c) CCT. (d) Conventional reduced-sized impedance transformer.

The length d of the transformer line in Fig. 5 is obtained from the point z'_L, the complex load re-normalized to Z'_0, and in the case of $\Gamma_r(r, x)|_{r_1} \leq 0$, they are

$$\tan(2\Theta_0) = \frac{\Gamma_i(r, x)|_{Z'_L}}{\Gamma_r(r, x)|_{Z'_L}} \tag{15}$$

in the case of $\Gamma_r(r, x)|_{r_1} \geq 0$ and $\Gamma_i(r, x)|_{Z'_L} \geq 0$, they are

$$\tan\left[2\left(\Theta_0 - \frac{\pi}{2}\right)\right] = \frac{\Gamma_i(r, x)|_{Z'_L}}{\Gamma_r(r, x)|_{Z'_L}} \tag{16a}$$

and in the case of $\Gamma_r(r, x)|_{r_1} \geq 0$ and $\Gamma_i(r, x)|_{Z'_L} \leq 0$, they are

$$\tan\left[2\left(\Theta_0 + \frac{\pi}{2}\right)\right] = \frac{\Gamma_i(r, x)|_{Z'_L}}{\Gamma_r(r, x)|_{Z'_L}} \tag{16b}$$

where $0 \leq \Theta_0 \leq \pi$ and $\Theta_0 = \beta d$ for an attenuation coefficient $\alpha \to 0$ and a phase coefficient $\beta = 2\pi/\lambda$.

B. CVT and CCT

2 : 1 quarter-wave impedance transformers are often utilized for 3-dB power dividers (ring hybrids and three-port power dividers). A 2 : 1 quarter-wave impedance transformer is plotted from 0.5 to 1 as a solid half-circle and a constant voltage standing-wave ratio (VSWR) circle passing through the point 0.5 is illustrated as a dotted half-circle in Fig. 6(a) in the case of an admittance Smith chart. To reduce the size of quarter-wave impedance transformers, it is necessary that the load admittance 0.5 be changed from a real into a complex admittance. For this, there are several possibilities. One of them is moving up along a constant VSWR circle, and another along a constant $g = 0.5$ circle, as indicated by the arrows in Fig. 6(a). The other cases, which are combined with the two methods, are also available, but for easy constructing of the transformers, the two methods will be discussed. The resulting circuit of the first method is shown in Fig. 6(b), that of second one is shown in Fig. 6(c). The transformer in Fig. 6(d) is a conventional reduced-sized transformer equivalent to a quarter-wave one [16]. By the background, the transmission-line transformer in Fig. 6(b) is named a CVT and that in Fig. 6(c) is named a CCT. Here, $\Theta_a + \Theta_b$ in the CVT or Θ_d in the CCT of Fig. 6 is much less than a quarter-wave. The graphs shown in Fig. 7(a) and (b) depict the impedance Z_b and length Θ_b of the CVT in Fig. 6(b) depending on Θ_a variations. Those in Fig. 7(c) and (d) also indicate the impedance Z_d and length Θ_d of the CCT in Fig. 6(c) depending on Θ_c variations. They have been produced based on (14) and (15). "IR 2.0," "IR 1.8," "IR 1.6," "IR 1.4," and "IR 1.2" in the graphs signify impedance transformation ratios. For these simulations, two impedances Z_a and Z_c are set to 50 Ω, and the reference impedance Z_r is also set to 50 Ω. Fig. 7(a) and (c) shows that, as the impedance transformation ratio goes higher, the impedance Z_b or Z_d also goes higher. The responses of Θ_b depending on Θ_a in Fig. 7(b) are almost linear in the CVT case. However, those of Θ_d depending on Θ_c in Fig. 7(d) are linear only in the case of the impedance transformation ratio IR greater than 1.6 and in the region of Θ_c smaller than 20°. The total length of the CVT is $\Theta_a + \Theta_b$, but that of the CCT is only Θ_d because the transmission line with Z_c is an open-circuited stub, and the open stub is easily substituted with a capacitor. As is well known, the conventional impedance transformer ability to match 100 to 50 Ω is its characteristic impedance 70.71 Ω and length 90°. This case is "IR 2," as shown in the graphs. The value for $\Theta_a = 0°$ or $\Theta_c = 0°$ in Fig. 7(a) or (c) is 70.7 Ω and the value for $\Theta_a = 0°$ or $\Theta_c = 0°$ in Fig. 7(b) or (d) is 90°. In this way, if the impedance transformation ratio is known, the impedance and length of the transformers are known with the variations of changed complex loads. The detailed data are tabulated in Tables II–V. A careful study of Tables IV and V in the case of IR = 1.6 shows that if $\Theta_c = 20°$, $Z_d = 95.92\ \Omega$ and $\Theta_d = 28.24°$. The fact indicates that a 1.6 : 1 transmission-line transformer can be realized with a transmission line 28.24° long together with a capacitor. Fig. 8 shows the frequency responses of reflected coefficients of CVTs and CCTs with IR = 1.6 on the basis of Tables II–V. For 1.6 : 1 impedance transformer realizations, the real load and reference impedance are set to 80 and 50 Ω, respectively. "CVT" and "CCT" on the graphs are CVTs and CCTs, and the following number denotes the electrical length of Θ_a and Θ_c in Fig. 6(b) and (c), respectively. These simulations have been carried out under ideal conditions, and CVTs and CCTs are designed at the center frequency of 3 GHz. From the simulated results, the reflection coefficients of all 1.6 : 1 impedance transformers at 3 GHz are between −73.36 to −94.259 dB. The frequency responses of "CVT 20°" and "CCT 10°" are about same with each other and that of "CCT 20°" is the worst case. Fig. 8(b) shows the comparison between the conventional transformers in Fig. 6(d) [16] and "CCT 20°" stated above. These simulations have been carried out under ideal conditions at the frequency of 3 GHz and the data for the simulations of the conventional transformers are when $\Theta = 28.24°$, $Z = 133.7\ \Omega$, and $C = 0.739$ pF, if $\Theta = 80°$, $Z = 64.22\ \Omega$, and $C = 0.146$ pF. The capacitance for the realization of the open-stub transmission line for "CCT 20°" is 0.39 pF. "Con" on the graph denotes the conventional transformers, and the following number is the length Θ of the transmission line in Fig. 6(d). The frequency responses of the "CCT 20°" are about same as those of the "Con 80°" from the simulated results in Fig. 8(b). The fact expresses that the length Θ in Fig. 6(d) must be greater than 80° in order that the

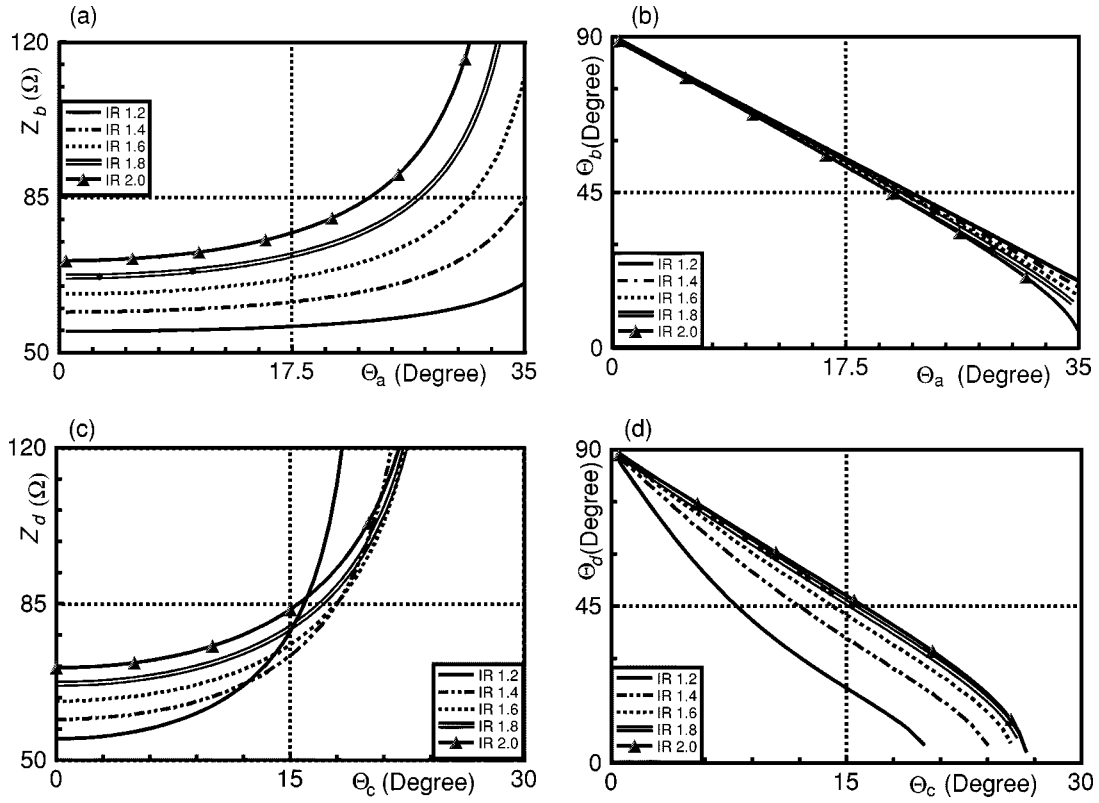

Fig. 7. Design graphs for CVT and CCT depending on impedance transformation ratios. (a) Impedance Z_b variation depending on Θ_a. (b) Length Θ_b variation depending on Θ_a. (c) Impedance Z_d variation depending on Θ_c. (d) Length Θ_b variation depending on Θ_c.

TABLE II
IMPEDANCE Z_b DEPENDING ON Θ_a

Θ_a	IR = 1.2	IR = 1.4	IR = 1.6	IR = 1.8	IR = 2.0
	Z_b / Ω, (Z_a = 50 Ω, Z_r = 50 Ω)				
0°	54.77	59.16	63.25	67.08	70.71
5°	54.85	59.32	63.48	67.40	71.12
10°	55.10	59.82	64.25	68.44	72.45
15°	55.55	60.76	65.70	70.44	75.03
20°	56.33	62.37	68.23	73.99	79.70
25°	57.65	65.19	72.80	80.63	88.80
30°	60.09	70.71	82.37	95.74	111.80
35°	65.65	85.16	113.45	166.95	440.86

TABLE III
LENGTH Θ_b DEPENDING ON Θ_a

Θ_a	IR = 1.2	IR = 1.4	IR = 1.6	IR = 1.8	IR = 2.0
	Θ_b / Degree, (Z_a = 50 Ω, Z_r = 50 Ω)				
0°	90°	90°	90°	90°	90°
5°	79.96°	79.86°	79.72°	79.56°	79.39°
10°	69.91°	69.70°	69.42°	69.09°	68.72°
15°	59.86°	59.53°	59.08°	58.55°	57.97°
20°	49.80°	49.31°	48.65°	47.88°	47.01°
25°	39.72°	39.02°	38.07°	36.93°	35.66°
30°	29.58°	28.56°	27.12°	25.35°	23.28°
35°	19.33°	17.63°	15.03°	11.31°	4.66°

performance of the conventional transformer can be equal to that of the "CCT 20°."

C. Microstrip CVTs and CCTs (1.6 : 1 Impedance Transformers)

On the basis of the derived design equations (14) and (15) and Tables II–V, 1.6 : 1 impedance transformers have been fabricated on an Al_2O_3 substrate ($\varepsilon_\gamma = 9.9$ and $h = 635$ μm) in microstrip technology. The layouts for the impedance transformers are depicted in Fig. 9 and the measured results are plotted in Fig. 10. These impedance transformers were designed at center frequency of 3 GHz and they are terminated in 80 and 50 Ω. Therefore, a quarter-wave impedance transformer to transform 80–50 Ω is additionally needed, and "Ipt" shown in Fig. 9 is the additional impedance transformer. A CVT 20°, CVT 30°, CCT 15°, and CCT 20° are illustrated in Fig. 9(a)–(d), respectively. The total length of the CVT 20° is 68.65°, that of CVT 30° is 57.12° from Table III, that of CCT 15° is 42.66°, that of CCT 20° is 28.24° from Table V. The measured results in Fig. 10 show very a similar tendency to those in Fig. 8(a). Since the reference impedance Z_r is 50 Ω in these small-sized impedance transformers, the characteristic impedances of Z_a and Z_c are all 50 Ω. The data for the fabrication of 1.6 : 1 microstrip impedance transformers are given in Table VI.

D. Bounded Length of CVT and CCT

In the case of the impedance transformation ratio $\mathrm{IR} = 2$, shown in Fig. 6(b)–(c), the locus of Θ_a or Θ_c starts from the point ($g = 0.5$, $b = 0$) on the real axis, as in Fig. 6(a), where g is a normalized conductance and b is a normalized susceptance.

TABLE IV
IMPEDANCE Z_d DEPENDING ON Θ_c

Θ_c	IR = 1.2	IR = 1.4	IR = 1.6	IR = 1.8	IR = 2.0
	Z_d / Ω, (Z_c = 50 Ω, Z_r = 50 Ω)				
0°	54.77	59.16	63.25	67.08	70.71
5°	56.35	60.30	64. 30	68.15	71.81
10°	62.17	64.26	67.91	71.75	75.57
15°	78.81	73.48	75.94	79.66	83.75
20°	254.87	99.88	95.92	98.54	103.131
25°			253.30	194.17	195.94

TABLE V
LENGTH Θ_d DEPENDING ON Θ_c

Θ_c	IR = 1.2	IR = 1.4	IR = 1.6	IR = 1.8	IR = 2.0
	Θ_d / Degree (Z_c = 50 Ω, Z_r = 50 Ω)				
0°	90	90	90	90	90
5°	59.39	69.73	73.30	74.98	75.89
10°	37.24	51.58	57.44	60.35	61.94
15°	21.54	35.96	42.66	46.16	48.09
20°	5.133	21.45	28.24	31.78	33.66
25°			9.70	13.79	15.30

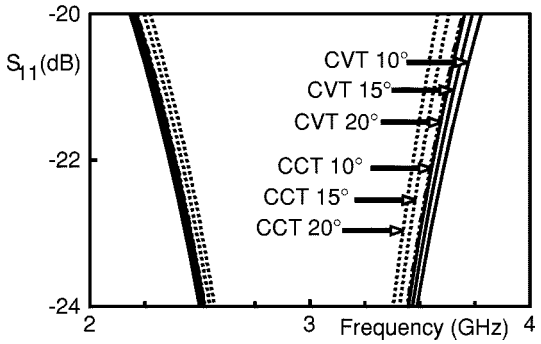

(a)

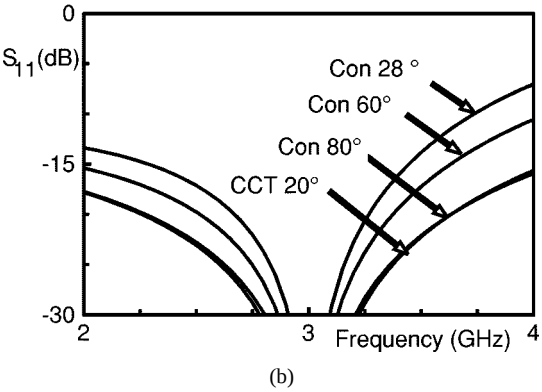

(b)

Fig. 8. Simulated matching results of impedance transformers for the impedance transformation ratio 1.6:1. (a) Simulated results of CVTs and CCTs ($Z_r = 50\,\Omega$). (b) Comparison between one CCT 20° and the conventional reduced-sized impedance transformers.

In the general case, the locus of Θ_a or Θ_c starts from the point ($g = 1/\mathrm{IR}$, $b = 0$) as the impedance transformation ratio IR is varied. When $g = 1/\mathrm{IR}$ and $b = 0$ on the Smith chart, the real part of the reflection coefficient at the point is $(\mathrm{IR}-1)/(1+\mathrm{IR})$, which is based on (11). In addition to that point, all constant conductance circles pass through a point $(1, 0)$ on the reflection-coefficient plane in Fig. 5. Therefore, the constant $g = 1/\mathrm{IR}$ circle is expressed as

$$\left(\Gamma_r - \frac{1}{\mathrm{IR}+1}\right)^2 + \Gamma_i^2 = \left(\frac{\mathrm{IR}}{\mathrm{IR}+1}\right)^2 \qquad (17)$$

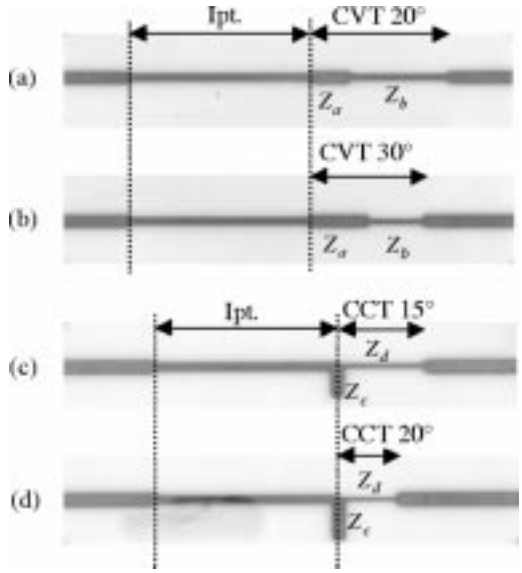

Fig. 9. Layouts for the microstrip small-sized 1.6:1 impedance transformers. (a) CVT 20°. (b) CVT 30°. (c) CCT 15°. (d) CCT 20°.

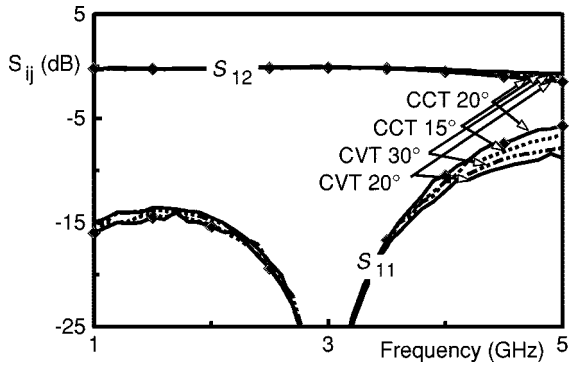

Fig. 10. Measured results of the microstrip small-sized 1.6:1 impedance transformers (CVT 20°. CVT 30°. CCT 15°. CCT 20°).

TABLE VI
FABRICATION DATA FOR THE MICROSTRIP 1.6:1 IMPEDANCE TRANSFORMERS
(w: WIDTH OF MICROSTRIP LINE, l: LENGTH OF MICROSTRIP LINE)

Ipt.		CVT 20°	CVT 30°
w = 356 um l = 9853 um	Z_a	w = 608 um	w = 608 um
	Θ_a	l = 2147 um	l = 3212 um
	Z_b	w = 292 um	w = 167 um
	Θ_b	l = 5357 um	l = 3025 um
Ipt.		CCT 15°	CCT 20°
w = 356 um l = 9853 um	Z_c	w = 607 um	w = 607 um
	Θ_c	l = 1610 um	l = 2147 um
	Z_d	w = 215 um	w = 98 um
	Θ_d	l = 4733 um	l = 3179 um

and the constant VSWR circle related with IR is

$$\Gamma_r^2+\Gamma_i^2=\left(\frac{1-\mathrm{IR}}{\mathrm{IR}+1}\right)^2. \tag{18}$$

These CVT and CCT are passive components. Therefore, the point r_1 in Fig. 5 must not be outside of $|\Gamma|=1$. For each locus of Θ_a or Θ_c to exist inside of $|\Gamma|=1$, two conditions must be satisfied and result in

$$\left(\Gamma_r+\frac{1}{2}\right)^2+\Gamma_i^2\le\left(\frac{1}{2}\right)^2 \tag{19}$$

$$\left(\Gamma_r-\frac{1}{2}\right)^2+\Gamma_i^2\le\left(\frac{1}{2}\right)^2. \tag{20}$$

The possible ranges of Θ_a and Θ_c are illustrated and a family of circles, a constant VSWR circle, a constant conductance circle, and two circles of (19) and (20) with "Im+" and "Im−" are drawn in Fig. 11(a). The family circles are phase angles between normalized voltages and currents with from 0° to 40° [17], and the center of the Smith chart in Fig. 11(a) is expanded in Fig. 11(b), where the changed complex loads of CVTs and CCTs designed in Fig. 8(a) are shown by dots. Here, the changed complex load of the CCT20° is located on the highest phase angle circle, whereas that of the CVT10° is on the lowest phase angle circle, and those of the CVT20° and CCT10° are on about the same phase angle circle. If the changed complex load is located on lower phase angle circle, the bandwidth is wider, as can be seen in Fig. 8(a). Therefore, the phase angle circles are related with a Q-factor and the bandwidth of the CVT10° shows the best performance among the small-sized transformers in Fig. 8(a). That means, depending on where the changed complex loads of the CVTs or CCTs are located, the relative bandwidth of CVTs and CCTs may be determined in Fig. 11(b), which agree with the results of Fig. 8(a).

The constant VSWR circle intersects two circles "Im+" and "Im−" at two points Θ_a^{m1} and Θ_a^{m2} in Fig. 11(b). Θ_a^{m1} is a maximum length of Θ_a in one region and Θ_a^{m2} a minimum length in another region. The formulas for Θ_a^{m1} and Θ_a^{m2} related with the impedance transformation ratio IR are

$$\tan\left[\pi-2\Theta_a^{m1}\right]=\frac{\Gamma_i^{m1}}{\Gamma_r^{m1}} \tag{21}$$

$$\tan\left[\pi-2\Theta_a^{m2}\right]=\frac{\Gamma_i^{m2}}{\Gamma_r^{m2}}=-\frac{\Gamma_i^{m1}}{\Gamma_r^{m1}} \tag{22}$$

where $\Gamma_r^{m1}=-(1-\mathrm{IR})^2/(\mathrm{IR}+1)^2$ and $\Gamma_i^{m1}=2(\mathrm{IR}-1)\sqrt{\mathrm{IR}}/(\mathrm{IR}+1)^2$ from (18)–(20). The constant $g=1/\mathrm{IR}$ circle intersects the circle "Im+" at only one point Θ_c^m in Fig. 11(b) and the imaginary part Γ_i^m for the Θ_c^m is $2\sqrt{\mathrm{IR}-1}/(\mathrm{IR}+3)$ from two circles in (17) and (19). The susceptance b for Γ_i^m is $\sqrt{\mathrm{IR}-1}/\mathrm{IR}$ from (12) and the transmission line with Z_c is the open-circuited stub in Fig. 6(c). Therefore, the length Θ_c^m is

$$\tan\left[\Theta_c^m\right]=\frac{\sqrt{\mathrm{IR}-1}}{\mathrm{IR}}. \tag{23}$$

From Fig. 11, the ranges where Θ_a exists are $0\le\Theta_a\le\Theta_a^{m1}$ and $\Theta_a^{m2}\le\Theta_a\le 90°$. Therefore, the CVT cannot be realized in the range between Θ_a^{m1} and Θ_a^{m2}, and those in Tables II–III and in Fig. 8(a) are all in $0\le\Theta_a\le\Theta_a^{m1}$. If Θ_a is greater than Θ_a^{m2}, the changed complex load of the CVT is located on the right-hand-side upper half-plane of the Smith chart and the length Θ_b is greater than 90° from (16a). Therefore, the CVTs with $\Theta_a^{m2}\le\Theta_a\le 90°$ may be realizable, but not recommendable. In the case of the CCTs, Θ_c is in one range $0\le\Theta_c\le\Theta_c^m$, as shown in Fig. 11(b). All data for Θ_a^{m1}, Θ_a^{m2} and Θ_c^m are written in Table VII as the impedance transformation ratio IR is varied.

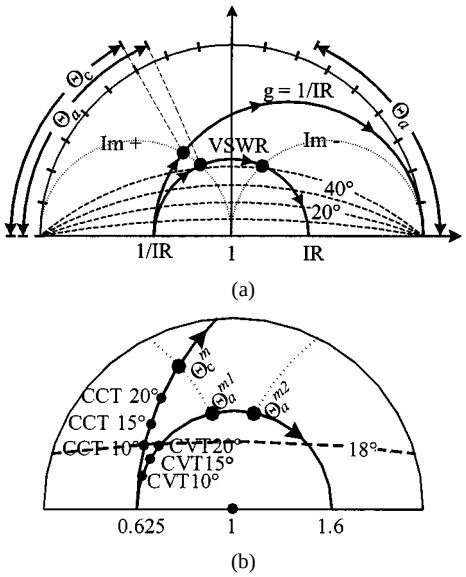

Fig. 11. Bounded lengths of Θ_a and Θ_c (a) Half of the Smith chart wherein a family of phase angle circles are drawn, illustrating the method to get the bounded lengths. (b) Loads of CVTs and CCTs with $\mathrm{IR}=1.6$ and the bounded lengths Θ_a^{m1}, Θ_a^{m2}, and Θ_c^m.

TABLE VII
BOUNDED LENGTHS OF CVTS AND CCTS

	$\Theta_a{}^{m1}$	$\Theta_a{}^{m2}$	$\Theta_c{}^{m}$
IR = 1.2	42.392°	47.608°	20.439°
IR = 1.4	40.203°	49.797°	24.311°
IR = 1.6	38.329°	51.671°	25.833°
IR = 1.8	36.699°	53.300°	26.423°
IR = 2.0	35.264°	53.736°	26.565°

IV. SMALL-SIZED THREE-PORT 3-dB POWER DIVIDERS

To reduce the size of a three-port power divider, the CVT and CCT are good candidates. Applying the CVT and CCT to conventional three-port 3-dB power dividers, the resulting circuits including the I.Cs are shown in Fig. 12. The three-port 3-dB power divider based on the CVTs is called a CVT3PD in Fig. 12(a) and that based on CCTs is called a a CVT3PD in Fig. 12(b), where Z_c' is $Z_c/2$.

A. I.Cs of the CVT3PD and CVT3PD

In the case of Fig. 12(a), the eigenadmittance y_1 [20] of the in-phase circuit contributed by the two ports ② and ③ without the I.C is

$$y_1=Y_{o/c}=Y_b\frac{Y_{\mathrm{CVT}oc}+jY_b\tan\Theta_b}{Y_b+jY_{\mathrm{CVT}oc}\tan\Theta_b} \tag{24}$$

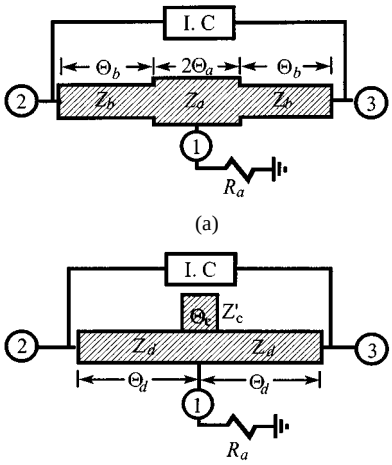

Fig. 12. Two-port circuits for the derivation of isolation conditions. (a) CVT3PD. (b) CCT3PD.

where $Y_a = 1/Z_a, Y_b = 1/Z_b$ and $Y_{\mathrm{CVT}oc} = Y_a(1 + j2R_aY_a \tan\Theta_a)/(2R_aY_a + j\tan\Theta_a)$, and the eigenadmittance y_2 of the out-of-phase circuit is

$$y_2 = Y_{s/c} = Y_b \frac{Y_{\mathrm{CVT}sc} + jY_b \tan\Theta_b}{Y_b + jY_{\mathrm{CVT}sc} \tan\Theta_b} \tag{25}$$

where $Y_{\mathrm{CVT}sc} = -jY_a \cot\Theta_a$.

For a perfect isolation between port ② and ③, shown in Fig. 12(a), the admittance parameter Y_{12} of all the circuit including the I.C must be zero, where the subscript of Y_{12} is not related with the port number, but related with a two-port circuit. Since the I.C is connected in parallel with the rest circuit, the impedance $Z_{\mathrm{I.C}}$ of the I.C in CVT3PD is $2/(y_1 - y_2)$ [13] and results in

$$Z_{I.C} = 2Z_b\left(\frac{Y_{\mathrm{CVT}oc}+jY_b\tan\Theta_b}{Y_b+jY_{\mathrm{CVT}oc}\tan\Theta_b} - \frac{Y_{\mathrm{CVT}sc}+jY_b\tan\Theta_b}{Y_b+jY_{\mathrm{CVT}sc}\tan\Theta_b}\right)^{-1}. \tag{26}$$

In the same way, the impedance $Z_{\mathrm{I.C}}$ of the I.C in CCT3PD of Fig. 12(b) is

$$Z_{I.C} = 2\left(Y_d\frac{Y_{\mathrm{CCT}oc} + jY_d\tan\Theta_d}{Y_d + jY_{\mathrm{CCT}oc}\tan\Theta_d} + jY_d\cot\Theta_d\right)^{-1} \tag{27}$$

where $Y_{\mathrm{CCT}oc} = 1/(2R_a) + j\tan\Theta_c/Z_c$, $Y_d = 1/Z_d$.

For $\Theta_a = 0°$, Θ_b is 90°, as shown in Table III. The value of $Z_{\mathrm{I.C}}$ for the case is Z_b^2/R_a in (26). In the case of conventional three-port 3-dB power dividers with $R_a = R_b = R_c = 50\ \Omega$, the impedance transformation ratio is two and the characteristic impedance of the $\lambda/4$ transmission line is $50\sqrt{2}\ \Omega$. Therefore, Z_b^2/R_a is 100 Ω in the case of $Z_b = 50\sqrt{2}\Omega$ and $R_a = 50\ \Omega$. The value 100 Ω is recognized as a well-known isolation resistance [1] in the conventional three-port 3-dB power dividers and coincides with $\Theta_c = 0°$ and $\Theta_d = 90°$ in (27). Two perfect isolation impedances have been simulated based on (26) and (27), and the results are plotted in Fig. 13, as Θ_a and Θ_c are varied. The perfect isolation impedance for the CVT3PD is plotted in

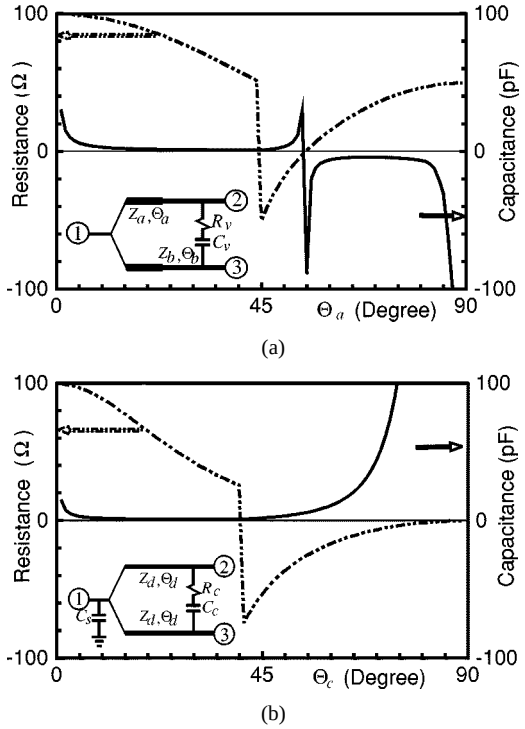

Fig. 13. Simulated results of two I.Cs of the CVT3PD and the CCT3PD. (a) Simulated results of the I.C for the CVT3PD. (b) Simulated results of the I.C for the CCT3PD.

Fig. 13(a) and that for the CCT3PD is plotted in Fig. 13(b). The left-hand-side axis of the two graphs in Fig. 13 indicates the real part of I.C with resistance Ω and the right-hand-side axis of the imaginary part of I.C with capacitance picofarad. The capacitance is calculated at the frequency of 3 GHz and R_a is set to 50 Ω. In the case of conventional three–port 3-dB power dividers terminated by equal impedances, the impedance transformation ratios IR_{12} and IR_{13} are equally two. Therefore, the 2 : 1 transformers have been used for CVT3PD and CCT3PD. In the two cases in Fig. 13(a) and (b), if Θ_a and Θ_c are equally 0°, the values for the both cases are equally 100 Ω, and if both Θ_a and Θ_c start to deviate from 0°, the capacitance starts to appear. If Θ_a is greater than Θ_a^{m1} ($\Theta_a^{m1} = 35.264°$ in Table VII) in Fig. 13(a), the characteristic impedance Z_b is imaginary from (14), but positive resistance still exists due to the termination impedance R_a and the transmission line with the characteristic impedance Z_a. If Θ_a is greater than 45°, the absolute of the negative resistance due to the imaginary characteristic impedance Z_b comes to be greater than that of the positive resistance due to the termination impedance R_a and the transmission line with Z_a. Therefore, the resulting value is negative up to Θ_a^{m2}. When Θ_a is equal to Θ_a^{m2}, the characteristic impedance of Z_b is 0 Ω and the resulting resistance of the I.C is 0 Ω. Therefore, the point where the resistance curve passes through 0 Ω is Θ_a^{m2}. Afterwards, positive resistance and negative capacitance appear. In the case, the total length of $\Theta_a + \Theta_b$ is greater than 90° and positive resistance together with inductance, which means the negative capacitance appears. As Θ_a is close to 90°, the characteristic impedance of Z_b is $50/\sqrt{2}\ \Omega$ and the resulting I.C is only a positive resistance 50 Ω. This case shows that a 2 : 1 impedance transformer may be realized with two transmission lines, which are each 90°

TABLE VIII
DESIGN DATA FOR CVT3PDs AND CCT3PDs

CVT3PD terminated by equal impedance 50 Ω at 3GHz
Z_a = 50 Ω, Θ_a = 29 °, Z_b = 104.8 Ω, Θ_b =25.9°
Z_{IC} = 76.5-j42.4 Ω → R_v =76.5 Ω, C_v = 1.25 pF
Z_a = 50 Ω, Θ_a = 20 °, Z_b = 79.7 Ω, Θ_b =47. °
Z_{IC} = 88.30-j 32.14 Ω → R_v = 88.30 Ω, C_v = 1.65 pF
CCT3PD terminated by equal impedance 50 Ω at 3GHz
Z_c = 50 Ω, Θ_c = 25 °, Z_d = 195.9 Ω, Θ_d = 15.3 ° C_s = 0.99 pF
Z_{IC} = 53.5-j 49.9 Ω → R_c = 53.5 Ω, C_c = 1.06 pF
Z_c = 50 Ω, Θ_c = 20 °, Z_d = 103.1 Ω, Θ_d = 33.66 ° C_s = 0.77 pF
Z_{IC} = 65.36-j 47.58 Ω → R_c =65.36 Ω, C_c = 1.11 pF

long and whose characteristic impedances are 50 Ω and $50/\sqrt{2}$ Ω, when the reference impedance $Z_r = 50\,\Omega$. The total length of the CVT3PD with $\Theta_a^{m2} \le \Theta_a \le 90°$ is much longer than that with $0 \le \Theta_a \le \Theta_a^{m1}$, but the CVT3PD with $0 \le \Theta_a \le \Theta_a^{m1}$ may be used in the case that the transmission lines with high characteristic impedance are not easily realized. On the other hand, since the available region of Θ_c for the CCT3PD is only $0 \le \Theta_c \le \Theta_c^m$, the positive resistance is bounded in one region, shown in Fig. 11(b), and when Θ_c is equal to Θ_c^m, the length of Z_d is 0° and the complex impedance of $Z_{\mathrm{I.C}}$ is $50 - j50\ \Omega$.

In conclusion, the two graphs in Fig. 13 show that the I.C must not only have resistance, but also inductance or capacitance for the perfect isolation in the case that the length of transmission lines is not $\lambda/4$.

B. Design of the CVT3PD and CCT3PD

On the basis of the derived isolation impedances, four cases of many possible designs are shown in Table VIII. These four examples are realizable in a practical case, and two cases have been simulated at the frequency of 3 GHz, and their results are plotted in Fig. 14. The results of the first CVT3PD in Table VIII are plotted in Fig. 14(a), and those of the first CCT3PD in Table VIII are plotted in Fig. 14(b). The design data for the CVT3PD as written in Table VIII are $Z_a = 50\,\Omega, \Theta_a = 29°, Z_b = 104.8\,\Omega$, $\Theta_b = 25.9°$, $R_v = 76.5\,\Omega$, and $C_v = 1.65$ pF in the inserted circuit in Fig. 13(a) and those of the CVT3PD are $Z_d = 195.9\,\Omega$, $\Theta_d = 15.3°$, $C_s = 0.99$ pF $R_c = 53.5\,\Omega$, and $C_c = 1.06$ pF in the inserted circuit in Fig. 13(b). In the two cases, the determination of the arbitrary design impedance A is not necessary, but the A is 50 Ω and only one in (1) and (2) because both of them are terminated by equal impedances 50 Ω's. The impedance transformation ratio IR_{12} or IR_{13} is equally two and always greater than one. Therefore, the results of S_{11} are worse than those of S_{22} or S_{33}. The performance of S_{23} may be improved more if another circuit, which has larger bandwidth, is replaced. The frequency responses of the CVT3PD are $|S_{12}| = |S_{13}| = -3.01$ dB, $|S_{11}| = -87.072$ dB, $|S_{23}| = -70.113$, $|S_{22}| = |S_{33}| = -70.085$ dB and those of the CCT3PD are $|S_{12}| = |S_{13}| = -3.01$ dB, $|S_{11}| = -58.945$ dB, $|S_{23}| = -70.261$, $|S_{22}| = |S_{33}| = -57.447$ at the center frequency of 3 GHz.

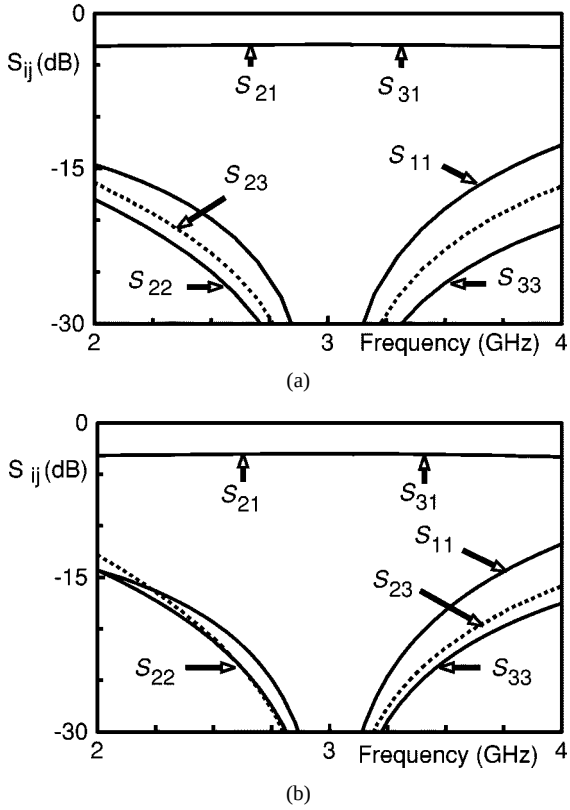

Fig. 14. Simulated results of a CVT3PD and CCT3PD terminated by equal impedance 50 Ω. (a) Simulated results of the CVT3PD. (b) Simulated results of the CCT3PD.

In this paper, only the examples with CCT3PD and CVT3PD are discussed, designed, and simulated. However, the concept of CCT3PD and CVT3PD may be extended to all possible cases of three-port power dividers with the general design equations. Therefore, any small-sized three-port power dividers may be obtained.

V. CONCLUSIONS

The three-port power divider with arbitrary power divisions terminated by arbitrary impedances considered in this paper is useful, not only for small-sized microwave circuit design, but also for easy design facilities due to as many sets of design equations as possible. Therefore, the design equations may be called general design equations and an arbitrary design impedance A is introduced to describe these general design equations. Additionally, to reduce the size of impedance transformers, two types of small-sized transmission-line impedance transformers CVT and CCT are designed. Finally, CVT3PD and CCT3PD are constructed based on CVTs and CCTs, and perfect isolation impedances are derived in the case that the length of transmission lines is not $\lambda/4$. Using the derived I.Cs, the perfect isolations are achieved for any available three-port power dividers, and allow to design small-sized CVT3PD and CCT3PD. In conclusion, general design equations, small-sized transformers, CVT3PDs, and CCT3PDs may play important roles in reducing the total size of MICs.

REFERENCES

[1] E. J. Wilkinson, "An n-way hybrid power divider," *IRE Trans. Microwave Theory Tech.*, vol. MTT-8, pp. 116–118, Jan. 1960.

[2] L. I. Parad and R. L. Moynihan, "Split-tee power divider," *IRE Trans. Microwave Theory Tech.*, vol. MTT-8, pp. 91–95, Jan. 1965.

[3] S. B. Cohn, "A class of broadband three-port TEM-mode hybrids," *IRE Trans. Microwave Theory Tech.*, vol. MTT-16, pp. 110–116, Feb. 1968.

[4] R. B. Ekinge, "A new method of synthesizing matched broad-band TEM-mode three-ports," *IEEE Trans. Microwave Theory Tech.*, vol. MTT-19, pp. 81–88, Jan. 1971.

[5] B. Kopp, "Asymmetric lumped element power splitters," in *IEEE MTT-S Int. Microwave Symp. Dig.*, vol. 1, 1989, pp. 333–336.

[6] D. Köther, B. Hopf, T. Sporkmann, and I. Wolff, "MMIC Wilkinson couplers for frequencies up to 110 GHz," in *IEEE MTT-S Int. Microwave Symp. Dig.*, vol. 2, 1995, pp. 663–665.

[7] S. Rosloniec, "Three-port hybrid power dividers terminated in complex frequency-dependent impedances," *IEEE Trans. Microwave Theory Tech.*, vol. 44, pp. 1490–1493, Aug. 1996.

[8] H. Hayashi, H. Okazaki, A. Kanda, T. Hirota, and M. Muraguch, "Millimeter-wave-band amplifier and mixer MMIC's using a broad-band 45° power divider/combiner," *IEEE Trans. Microwave Theory Tech.*, vol. 46, pp. 811–818, June 1998.

[9] H.-R. Ahn, I.-S. Chang, and S.-W. Yun, "Miniaturized 3-dB ring hybrid terminated by arbitrary impedances," *IEEE Trans. Microwave Theory Tech.*, vol. 42, pp. 2216–2241, Dec. 1994.

[10] H.-R. Ahn, I. Wolff, and I.-S. Chang, "Arbitrary termination impedances, arbitrary power division and small-sized ring hybrids," *IEEE Trans. Microwave Theory Tech.*, vol. 45, pp. 2241–2247, Dec. 1997.

[11] H.-R. Ahn and I. Wolff, "3-dB branch-line hybrid terminated by arbitrary impedances," *Electron. Lett.*, vol. 34, no. 11, pp. 1109–1110, May 1998.

[12] ——, "Asymmetric four-port and branch-line hybrids," *IEEE Trans. Microwave Theory Tech.*, vol. 48, pp. 1585–1588, Sept. 2000.

[13] ——, "Three-port 3-dB power divider terminated by different impedances and its application to MMIC's," *IEEE Trans. Microwave Theory Tech.*, vol. 47, pp. 786–794, June 1999.

[14] ——, "General design equations of three-port unequal power dividers terminated by arbitrary impedances," in *IEEE MTT-S Int. Microwave Symp. Dig.*, vol. 2, 2000, pp. 1137–1140.

[15] G. N. French and E. H. Fooks, "The design of stepped transmission line transformers," *IEEE Trans. Microwave Theory Tech.*, vol. MTT-16, pp. 885–886, Oct. 1968.

[16] T. Hirota, A. Minakawa, and M. Muraguchi, "Reduced-size branch-line and rat-race hybrids for uniplanar MMIC's," *IEEE Trans. Microwave Theory Tech.*, vol. 38, pp. 270–275, Mar. 1990.

[17] P. H. Smith, *Electronic Applications of the Smith Chart*. New York: McGraw-Hill, 1969, pp. 38–39.

[18] M. A. Hamid and M. M. Yunik, "On the design of stepped transmission-line transformers," *IEEE Trans. Microwave Theory Tech.*, vol. MTT-15, pp. 528–529, Sept. 1967.

[19] G. D. Vendelin, A. M. Pavio, and U. L. Rohde, *Microwave Circuit Design Using Linear and Nonlinear Techniques*. New York: Wiley, 1990, pp. 163, 172–173.

[20] J. Helszajn, *Passive and Active Microwave Circuits*. New York: Wiley, 1978, p. 37.

Hee-Ran Ahn (S'90–M'95–SM'99) received the B.S., M.S., and Ph.D. degrees in electronic engineering from Sogang University, Seoul, Korea, in 1988, 1990, and 1994, respectively, and is working toward the Habilitation degree at Gerhard-Mercator University Duisburg, Duisburg, Germany.

From 1991 to 1995, she was a Part-Time Lecturer at Sogang University, and a Post-Doctoral Fellow from 1996 to 1997. Since February 1997, she has been with the Institute of Electromagnetic-Field Theory, Department of Electrical Engineering, Gerhard-Mercator University Duisburg. Her current interests include high-frequency circuit designs.

Ingo Wolff (M'75–SM'85–F'88) was born in Koeslin, Germany, on September 27, 1938. He received the Dipl.-Ing., Dr.-Ing., and Habilitation degrees from the Technical University Aachen, Aachen, Germany, in 1964, 1967, and 1970, respectively.

In 1974, he became the Chair of Electromagnetic Field Theory at Duisburg University, Duisburg, Germany. He remained in that position until 1999. Since 1999, he has been the President of Duisburg University, Duisburg, Germany. In 1992, he founded and is currently the Managing Director of the Institute of Mobile and Satellite Telecommunications (IMST), Kamp-Lintfort, Germany, a private research institute for wireless communication techniques in which over 110 coworkers are involved in research and development.